Open access • Journal Article • DOI:10.1021/ACSNANO.8B07578

Single Nanocrystal Spectroscopy of Shortwave Infrared Emitters — Source link

Sophie N. Bertram, Boris Spokoyny, Daniel Franke, Justin R. Caram ...+4 more authors

Institutions: Massachusetts Institute of Technology, University of California, Los Angeles

Published on: 30 Nov 2018 - ACS Nano (American Chemical Society)

Topics: Nanocrystal, Indium arsenide and Spectroscopy

Title
Single Nanocrystal Spectroscopy of Shortwave Infrared Emitters.

Journal
ACS nano, 13(2)

ISSN
1936-0851

Authors
Bertram, Sophie N
Spokoyny, Boris
Franke, Daniel
et al.

Publication Date
2019-02-01

DOI
10.1021/acsnano.8b07578

Peer reviewed

ACS NANO
Cite This: ACS Nano 2019, 13, 1042−1049
www.acsnano.org

ARTICLE

Single Nanocrystal Spectroscopy of Shortwave Infrared Emitters

Sophie N. Bertram,[†,⊥] Boris Spokoyny,[†,⊥] Daniel Franke,[†] Justin R. Caram,[‡] Jason J. Yoo,[†] Ryan P. Murphy,[§] Matthew E. Grein,[§] and Moungi G. Bawendi*[,†]

[†]Department of Chemistry, Massachusetts Institute of Technology, 77 Massachusetts Avenue, Cambridge, Massachusetts 02139, United States

[‡]Department of Chemistry, University of California, Los Angeles, 607 Charles E Young Drive E, Los Angeles, California 90095, United States

[§]MIT Lincoln Laboratory, 244 Wood Street, Lexington, Massachusetts 02421, United States

Supporting Information

ABSTRACT: **Short-wave infrared (SWIR) emitters are at the center of ground-breaking applications in biomedical imaging, next-generation optoelectronic devices, and optical communications. Colloidal nanocrystals based on indium arsenide are some of the most promising SWIR emitters to date. However, the lack of single-particle spectroscopic methods accessible in the SWIR has prevented advances in both nanocrystal synthesis and fundamental characterization of emitters. Here, we demonstrate an implementation of a solution photon correlation Fourier spectroscopy (s-PCFS) experiment utilizing the SWIR sensitivity and time resolution of superconducting nanowire single-photon detectors to extract single-particle emission linewidths from colloidal indium arsenide/cadmium selenide (InAs/CdSe) core/shell nanocrystals emissive from 1.2 to 1.6 μm. We show that the average single InAs/CdSe nanocrystal fluorescence linewidth is, remarkably, as narrow as 52 meV, similar to what has been observed in some of the most narrowband nanostructured emitters in the visible region. Additionally, the single nanocrystal fluorescence linewidth increases with increasing shell thickness, suggesting exciton−phonon coupling as the dominant emission line-broadening mechanism in this system. The development of the SWIR s-PCFS technique has enabled measurements of spectral linewidths of colloidal SWIR-emissive NCs in solution and provides a platform to study the single NC spectral characteristics of SWIR emitters.**

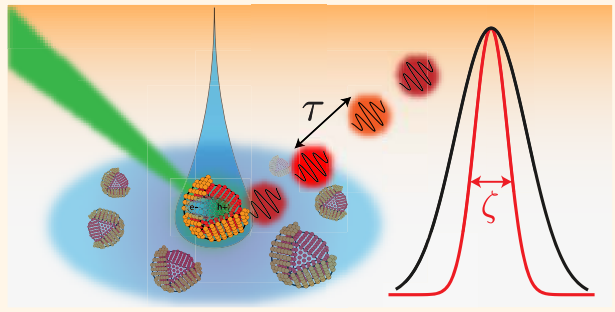

KEYWORDS: *nanocrystals, single-molecule spectroscopy, short-wave infrared, indium arsenide, core/shell*

Traditionally, the short-wave infrared (SWIR) region of the electromagnetic spectrum (1−2 μm) has been restricted to very few applications. Most notably, modern optical telecommunication operates almost exclusively in the SWIR due to the low Rayleigh scattering cross section of silica-based optical fibers and the high-power transmission achievable in certain spectral windows (*e.g.*, 1530−1565 nm C-band used for telecommunications) due to the relatively weak water absorption in those regions.[1] However, recent advances in materials science and detector technology have opened up the SWIR region to a variety of diverse applications. These advances have found their way into biomedical imaging applications, where in contrast to visible−near-IR (vis−NIR) emitters, SWIR-emitting biomarkers show improved imaging contrast and resolution due to inherently lower tissue scattering and deeper penetration depths.[2−4] Synthesis of infrared-emitting colloidal quantum dots has led to the development of a wide range of emerging technologies from quantum dot light-emitting diodes (QD-LEDs) to on-chip biosensing and solution-processable photodetectors.[5−11] The development of superconducting nanowire single-photon detectors (SNSPDs), which boast some of the highest sensitivities, the highest time resolution, and lowest noise of any SWIR single-photon detector technology, has enabled applications ranging from deep-space high-rate optical communications, to high-resolution imaging, quantum optics, and quantum networks.[12−15] Whereas a host of potential single-visible-photon emitters have been studied, producing single-photon emitting materials for the SWIR that are

Received: October 4, 2018
Accepted: November 26, 2018
Published: November 30, 2018

DOI: 10.1021/acsnano.8b07578
ACS Nano 2019, 13, 1042−1049

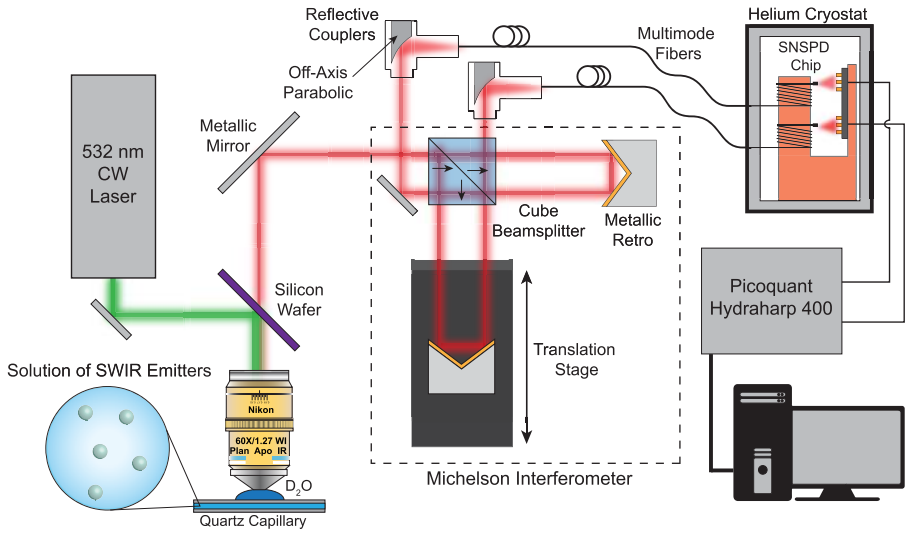

Figure 1. SWIR s-PCFS setup. InAs/CdSe NCs diffusing freely in solution are photoexcited with a 532 nm CW laser (CrystaLaser) focused to a diffraction-limited spot with a 60× Nikon objective. The emitted photons are collected through the same objective and passed through a silicon wafer acting as a dichroic mirror to filter out excitation light. The SWIR photons are passed through a Michelson interferometer, where each arm is coupled into a 30 μm core multimode fiber and sent to the SNSPDs. Photon time tags are recorded with a time-correlated photon counting device (Picoquant, HydraHarp 400) and sent to a PC for analysis.

compatible with the existing telecommunications band remains an outstanding challenge.[16,17]

The most promising SWIR-emissive materials that have been developed to date include carbon nanotubes, rare-earth-doped phosphors, organic dyes, and semiconducting nanocrystals (NCs).[18−22] Semiconducting NCs are remarkable because they are highly photostable, solution-processable, and exhibit photoluminescence quantum yields (PLQYs) orders of magnitude higher than those of their organic analogues.[23] Among narrow band gap NCs, materials composed of lead chalcogenides (PbX; X = S, Se, Te) and indium arsenide (InAs) have the highest reported PLQYs with PbS ranging from 60% at 1 μm to 30% at 1.5 μm and InAs ranging from as high as 37% at 1 μm to 16% at 1.5 μm.[24,25]

In addition to a high PLQY, another sought after spectral characteristic for these materials is a narrow fluorescence linewidth. For applications such as multicolor fluorescence imaging or frequency-division multiplexing, narrow emission linewidths facilitate the tight spectral discrimination that is required to achieve a high signal-to-noise ratio (SNR).[26,27] From a fundamental standpoint, fluorescence linewidths can elucidate the nature of the energy landscape of the material and the coupling between the exciton and its environment. For NCs, in particular, the ensemble fluorescence linewidth is the convolution of the emission linewidths of all individual NCs. The lifetime-limited spectrum of individual NCs can be broadened by a variety of interactions such as exciton−phonon coupling, spectral diffusion, or exciton fine structure.[28,29] Understanding these mechanisms requires reliable characterization of the individual nanoparticle optoelectronic properties.

A variety of established single-molecule spectroscopic techniques are routinely used in the vis−NIR part of the electromagnetic spectrum to elucidate the fundamental physical mechanisms governing the emission line shape. Single-molecule confocal microscopy has been a ubiquitous tool in spectroscopic studies of a variety of visible emitters.[30,31] In this technique, a film of well-separated NCs is photoexcited, and emission from a single NC is collected through a confocal microscope and subsequently spectrally analyzed. One of the potential downsides of this approach is that the NCs are fixed to a solid-state substrate and are no longer interrogated in their native solution environment. Because the spectral line shape and the PLQY of each nanoparticle could be altered by the presence of the substrate, it is crucial to carry out spectral characterization in solution.[32] This becomes especially important for biomedical applications, where the NCs acting as biomarkers are suspended in liquid media.[26,33] Another drawback comes from the inherent bias in selecting NCs for characterization. Obtaining a single NC spectrum requires integrating enough signal from a single NC to obtain a good SNR. Statistically, only the brightest NCs emit enough photons to collect a spectrum, leading to the interrogation of only the most stable and emissive NCs.

The development of s-PCFS addresses concerns with traditional NC spectroscopy by performing single NC measurements in solution, utilizing high-speed single-photon time-tagging hardware to discriminate photons coming from single NCs diffusing through the interrogated focal volume.[34] In a s-PCFS experiment, emission from a dilute solution of freely diffusing NCs is collected in a confocal microscope setup, sent through a Michelson interferometer, and detected by a pair of single-photon detectors (see Figure 1). The intensities at each output of the interferometer are correlated to separate pairs of photons with different lag times such that, after subtracting ensemble contributions, photons with lag time shorter than the diffusion time of the particle through the focal volume can be assigned to a single emitter. Conversely, pairs of photons with lag times longer than the diffusion time of the particle through the focal volume can be assigned to different emitters. By collecting photon streams at different interferometric positions inside and outside of the coherence length of the emitter, we can extract the average single NC ($p^{\text{single}}(\zeta,\tau)$) and the ensemble spectral correlations ($p^{\text{ensemble}}(\zeta,\tau)$), where ζ is the energy difference between the photons and τ is the lag time between the arrival times of the photons. The key feature—and drawback—of s-PCFS is that even though it

DOI: 10.1021/acsnano.8b07578
ACS Nano 2019, 13, 1042−1049

interrogates every NC coming into the focal volume, the technique sacrifices information about the absolute energy of each detected photon, instead producing a tally of all photon energy differences. The advantage of this approach is that it no longer necessitates long integration times for each NC—as long as the emitter generates at least two photons while inside the focal volume, its contribution to the average single-particle linewidth will be recorded. Formally, the resulting s-PCFS trace is an averaged autocorrelation of the absolute single-particle spectrum.

At its core, s-PCFS is a confocal microscopy technique that relies on faithful imaging of the sample plane onto the conjugate plane of the pinhole. This pinhole serves to reject stray light and provides a well-defined sample interrogation volume.[35] Because s-PCFS also extracts spectral information, great care must be taken to ensure that the spectrum of light emitted from the sample is not altered by the collection optics. Most commercial optical components such as high-NA objectives and lenses are optimized for the visible, posing a significant challenge when designing systems in the SWIR. Most visible optics exhibit significant transverse and longitudinal chromatic aberrations (TCAs and LCAs) when used in the SWIR, leading to spatial blurring and reduced spectral transmission through the confocal pinhole (Figure 2a). Fluorescence correlation experiments like s-PCFS rely on intensity fluctuations in the emitted photon stream. The presence of focal volume distortions and chromatic aberrations leads to a decrease in the average fluctuation amplitude which manifests itself as an inflated occupation volume and significantly decreased correlation curve SNR (Figure 2b).

Due to these difficulties, single NC spectral characterization of red emitters has been limited to NIR-emissive PbS, and most to-date studies of SWIR emitters have been limited to investigations of the fluorescence intermittency patterns and characteristic fluorescence lifetimes.[36−38] Although there has been some work assessing spectral linewidths of colloidally prepared SWIR-emitting PbS nanocrystals and epitaxially grown InAs in the solid state, no work exists on SWIR-emitting nanocrystals in their native solution environment.[39,40]

Traditionally, spectroscopic setups in the IR have circumvented these issues by employing all-reflective designs, including reflective objectives based on a two-mirror Schwarzschild design.[41] However, in a Schwarzschild objective, the secondary mirror sits in the light path of the primary mirror, creating a central obscuration in the far-field beam. This annular beam, while free of chromatic aberrations, cannot be efficiently coupled through a circular aperture of a confocal pinhole. Moreover, reflective objectives with a higher NA have larger central obscurations, leading to even poorer coupling that reaches theoretical efficiencies of 10% for a 0.8 NA objective.[42,43] Therefore, our application requires the use of refractive, IR-compensated objectives. Figure 2c shows experimental spectral transmission data using three commercially available objectives. A broadband superluminescent diode (SLD) with a bandwidth full width at half-maximum (FWHM) of 100 nm centered at 1.55 μm (solid black curve) was reflected from a gold mirror positioned at the sample plane and imaged onto the entrance of a single mode fiber coupled to a spectrum analyzer (Agilent 861140b). We see that the collection optics greatly influence the SWIR spectral transmission. Using a visible oil-immersion objective with SWIR light leads to severe spectral filtering through the confocal pinhole (single-mode fiber), whereas the use of a reflective

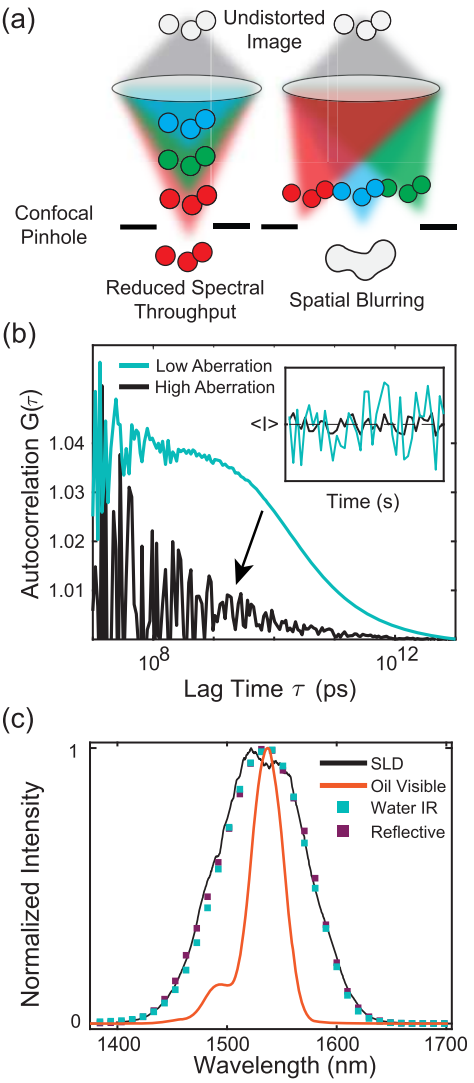

Figure 2. (a) Cartoon showing the effect of spectral filtering and blurring that occurs in confocal setups in the presence of chromatic aberrations. (b) Schematic influence of chromatic aberrations on s-PCFS data quality. Blurring reduces the amplitude of intensity fluctuations, lowering the overall SNR. (c) Spectral transmission of a superluminescent diode (FWHM = 100 nm) through the setup using different focusing objectives. The visible oil-immersion objective shows significant spectral filtering (cutoff).

objective (Thorlabs LMM-40X-P01) or a chromatically corrected IR objective (Nikon 60× Plan Apo IR) leads to satisfactory spectral transmission.

Another salient feature of the SWIR s-PCFS setup in Figure 1 lies on the detection side. The correlation-based measurements used in s-PCFS necessitate sensitive, fast, single-photon detectors. Whereas this technology is ubiquitous for visible light detection, single-photon detectors sensitive in the SWIR have only recently been developed. The niobium nitride (NbN)-based SNSPD detectors used in our experiments are similar to those described previously.[37,38,44] Light is collected in an optical fiber and focused onto a 14 μm diameter SNSPD through the backside of a thick (~250 μm) silicon substrate with an actively positioned dual lens asphere assembly. A weak optical cavity around the thin NbN nanowires is optimized for peak absorption of 1550 nm photons to yield a peak efficiency

DOI: 10.1021/acsnano.8b07578
ACS Nano 2019, 13, 1042−1049

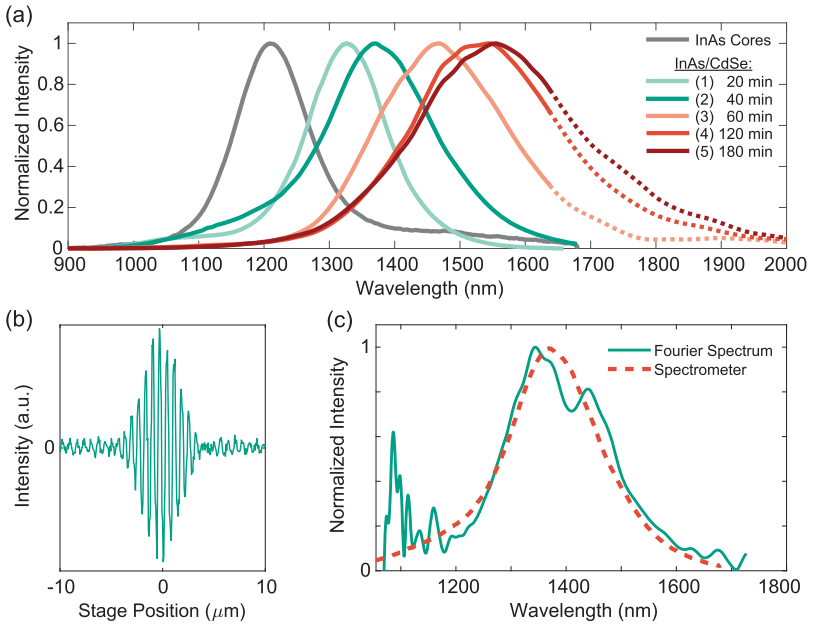

Figure 3. (a) Ensemble fluorescence spectra of the InAs/CdSe core−shell series. Due to the limited detector bandwidths, the spectra were stitched together from measurements on two different detectors (thin InGaAs detector (solid), extended InGaAs detector (dashed)). (b) Example interferogram obtained in the SWIR s-PCFS setup. (c) Fourier spectrum obtained in the SWIR s-PCFS setup (solid) and in a grating spectrometer (dashed), showing good agreement. The slight depression in the Fourier spectrum at ∼1380 nm stems from water absorption in the fibers leading to the SNSPDs.

of ∼65%, and the 1.17 eV silicon band gap acts as a long-pass filter for light to the red of 1050 nm (see Figure S1 in the Supporting Information). The light collection fibers are specially designed multimode, weakly polarization-maintaining, graded index optical fibers with a 0.2 numerical aperture and a 30 μm core diameter. The 30 μm core of the multimode fiber acts as the confocal pinhole in our experiments.[45]

RESULTS AND DISCUSSION

To demonstrate the efficacy of our SWIR s-PCFS system, we studied single nanoparticle linewidth properties of InAs/CdSe quantum dots emitting in the 1.2−1.6 μm region. The synthesis of InAs NCs was originally described decades ago, in which core-only InAs NCs showed extremely low PLQYs. It was later shown that the addition of an inorganic shell composed of ZnCdS or CdSe significantly improves the PLQY, likely due to increased surface charge passivation.[46,47] However, synthesis of InAs NCs exhibiting efficient emission in the SWIR remained a challenge. Combating the difficult chemistry associated with III−V semiconductor NCs, our group has recently gained kinetic control of the core growth by tuning the rate of precursor addition, yielding higher PLQY particles and allowing for longer shell growth and redder emission wavelengths.[25] InAs/CdSe NCs have a quasi-type-II band structure where the hole wave function is confined to the core and the electron wave function delocalizes over the core and the shell. In these systems, growth of the shell leads to a red shift in the emission maximum due to increased electron delocalization.[48] Here, we synthesized InAs NC core particles emissive at 1200 nm and used a continuous injection of the Cd and Se precursors to grow a CdSe shell. Aliquots were taken at 20, 40, 60, 120, and 180 min of shell growth time (samples 1−5, from now on), resulting in NC emission ranging from 1200 to 1590 nm, as summarized in Figure 3a. Absorption spectra and transmission electron microscopy (TEM) images of the synthesized particles can be found in Figure S2 along with the corresponding PL lifetimes in Figure S3. The ensemble PL shows a relatively broad emission across the SWIR with FWHM ranging from 100 to 150 meV. To verify the spectral transmission through the SWIR s-PCFS setup, we performed interferometric measurements of the ensemble InAs/CdSe spectra. Figure 3b shows a typical interferogram from the concentrated InAs/CdSe (2) sample obtained by scanning the translation stage of our Michelson interferometer and integrating emission for 100 ms per step using our SNSPDs. In order to minimize absorption from CH and OH stretches in the spectral window of the NC emission, the NCs were suspended in tetrachloroethylene (TCE), and we used deuterated water (D_2O) as the immersion medium for the IR compensated objective. Figure 3c plots the discrete Fourier transform (DFT) of the interferogram in (b) and overlays it with the ensemble spectrum from (a). The spectrum of the broad NC emission obtained in our s-PCFS setup reproduces the IRPL data quite well. The small dip at ∼1380 nm results from water absorption in the multimode fibers leading into the SNSPDs and any other transmissive silica optics.[49]

To investigate the single-particle properties, we first performed an s-PCFS measurement on the InAs/CdSe sample with the thinnest shell (light green in Figure 3a). We were not able to perform single-particle characterization on the InAs cores due to the low QY of the unshelled NCs and the spectral cutoff of the SNSPDs. The stock solution of NCs was diluted in TCE to obtain a focal occupation of ∼25 particles (see representative fluorescence correlation spectroscopy (FCS) trace in the Supporting Information, Figure S4). At lower concentrations, the emissive properties of the NC solution quickly degraded likely due to a loss of colloidal stability. Figure 4a shows the averaged single and ensemble NC linewidths (blue and black lines, respectively) for the InAs/CdSe samples with the bluest emission (InAs/CdSe (1) in

DOI: 10.1021/acsnano.8b07578
ACS Nano 2019, 13, 1042−1049

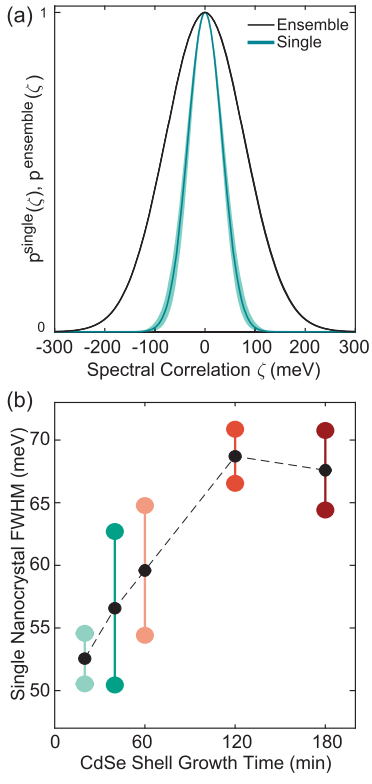

Figure 4. (a) Gaussian fits of the single InAs/CdSe (1) NC (blue) and ensemble (black) spectral correlations. Error in the single NC spectral correlation is shown in light blue around the average single NC spectral correlation. (b) Evolution of the InAs/CdSe (1−5) shell series spectral correlation fwhm as a function of CdSe shell thickness. The linewidth values were extracted by fitting the single-particle spectral correlations to a single Gaussian, extracting the fwhm, and dividing by the Gaussian deconvolution factor ($\sqrt{2}$). For each shell thickness, two separate measurements of the single NC spectral correlation fwhm are shown with the colored data points, with the average shown in black.

Figure 3a). The ensemble linewidth predictably reproduces the width obtained from the IRPL measurements (~100 meV), whereas the averaged single-particle linewidth appears to be almost twice as narrow (~52 meV) as the ensemble linewidth. This discrepancy between ensemble and single NC linewidth suggests that there is significant inhomogeneous broadening in this system in contrast to NIR-emissive PbS NCs, which show single NC linewidths of ~180 meV dominated by homogeneous broadening.[36] Remarkably, the single NC linewidth of InAs/CdSe is comparable to some of the narrowest visible CdSe NCs, with room temperature emission linewidths ranging from 40 to 70 meV.[50] In addition, visible-emissive InAs/ZnS NCs have single NC linewidths on the order of 70−80 meV, suggesting that, intrinsically, the InAs/CdSe NCs are significantly narrower.[50]

To investigate the single NC linewidth evolution as a function of shell thickness in InAs/CdSe, we performed s-PCFS measurements on the remaining, redder-emitting NC samples. The trend in single NC linewidths is shown in Figure 4c. We see that, in general, the single NC linewidth increases with shell growth and appears to plateau for the largest shell sizes. For quasi-type-II heterostructures, like InAs/CdSe, the broadening of the single-particle linewidths with increasing shell thickness is commonly attributed to enhanced exciton−phonon coupling (EPC).[28,50] However, there is little consensus in the literature on how the magnitude of EPC evolves with shell thickness. Some single-particle studies on CdSe/CdS core−shell structures show a continuous increase in single-particle linewidth and attribute it to a steady increase in EPC with shell thickness.[28,50] While other studies on the same material, using resonance Raman techniques shows slight reductions in EPC upon growth of a CdS shell onto CdSe core NCs.[51] The predominant mechanism of EPC in type-II heterostructures is thought to be polar (Fröhlich) coupling between the electric field induced by the separated electron and hole (exciton) and the oscillating dipole moment created by an LO phonon.[52] Qualitatively, Fröhlich coupling is proportional to (1) the LO phonon wavelength (inversely proportional to LO wavevector) and (2) the degree of electron−hole wave function delocalization. Therefore, the strength of EPC can be governed by mechanisms that scale oppositely with shell growth. For example, an increase in shell size both decreases the LO phonon wavelengths due to phonon confinement effects (decrease in EPC) and increases the degree of electron−hole wave function delocalization (increase in EPC).[50,53] Other competing considerations such as the influence of the excitation wavelength on the LO phonon wavelength can also play a significant role in the EPC and subsequently the NC linewidth trend.[51,53] Combining all of these effects, it is likely that in our system, there are several competing processes that lead to the observed initial increase and subsequent plateauing of the single-particle linewidth for the largest shell sizes. Future work on temperature-dependent linewidths of individual InAs/CdSe NCs will be able to provide a more quantitative picture of the role of shell thickness on EPC for SWIR-emitting quasi-type-II heterostructures.

CONCLUSIONS

In summary, we have presented spectral characterizations of single colloidal SWIR emitters in their native solution environment using an implementation of s-PCFS that utilizes SWIR corrected optics and SNSPD detectors. Our results indicate that preparation of InAs/CdSe NCs for SWIR applications are not fundamentally limited by the line width or the intrinsic properties of the emitter but rather by the methods by which the emitters are synthesized. Using s-PCFS, we have shown that the linewidth of single InAs/CdSe NCs can be as narrow as ~52 meV and increases to ~70 meV for the reddest emitting samples, likely due to exciton−phonon-mediated broadening mechanisms. This insight highlights the importance of fundamental dissipation mechanisms in determining the optoelectronic properties of SWIR emitters and establishes avenues toward synthetic optimization of these materials.

METHODS

InAs NC Synthesis. InAs cores and InAs/CdSe core/shell samples (1−5) were synthesized according to protocols outlined in ref 25. The indium precursor was prepared by dissolving indium(III) acetate in oleic acid and octadecene (ODE) in a four-necked flask. This solution was degassed at room temperature for 5 min and further degassed at 115 °C for 60 min. The solution was then heated to 295 °C. Tris(trimethylsilyl) arsine ($(TMSi)_3As$) in trioctylphosphine (TOP) was dissolved and loaded into the injection syringe. This solution was injected into the indium solution and allowed to react for 10 min. After the hot injection process, we continuously injected a solution of tris(trimethylgermyl)arsine ($(TMGe)_3As$) in ODE at a rate of 2 mL/h for the first 30 min of the reaction and then at a rate of 0.15 mL/h

DOI: 10.1021/acsnano.8b07578
ACS Nano 2019, 13, 1042−1049

for 4 h more. In order to grow a CdSe shell on the InAs core particles, the InAs cores were degassed at room temperature for 60 min and subsequently heated to 110 °C for 10 min under vacuum. The cadmium precursor was prepared by combining cadmium oxide with oleic acid to form cadmium oleate ($Cd(Ol)_2$). The selenium precursor was prepared by combining TOP and selenium to form a solution of TOPSe and further mixed with ODE. Once the precursors were prepared, the InAs core solution was heated to 280 °C, and once the mixture reached 240 °C, the shell precursor injection was initiated. The ($Cd(Ol)_2$) and TOPSe solutions were injected at a rate of 2 mL/h. Aliquots were pulled at 20, 40, 60, 120, and 180 min after the start of the shell injection.

Ensemble IRPL. The ensemble emission spectra were taken on a home-built infrared PL setup equipped with a grating monochromator and a thin InGaAs detector (Thorlabs DET10N).

s-PCFS Experiment. The output of a continuous wave 532 nm laser (Crystalaser CL532-025-S) was coupled into a single-mode fiber, and its output was collimated using an 8.5 mm diameter reflective collimator (Thorlabs RC08FC-P01) serving as the excitation source in our experiment. The 532 nm excitation was attenuated to ∼20 μW with a neutral density filter, reflected from a silicon wafer that served as a long-pass dichroic mirror, and was focused inside the sample-containing quartz capillary with an IR corrected water-immersion objective (Nikon CFI Plan Apo IR SR 60XWI). Deuterated water was used as the immersion medium. The collected fluorescence passed through the silicon dichroic and was directed to a Michelson interferometer. The emission was split into two arms with a nonpolarizing cube beamsplitter (Thorlabs BS033), and the distance in one of the arms was varied using a motorized stage (Aerotech Ensemble ANT95-100-L). The emission in the interferometer arms was then coupled into two 30 μm core diameter multimode fibers using a pair of off-axis parabolic mirrors (Thorlabs RC08FC-P01). A detailed description of the SNSPD detectors used in the experiment can be found in ref 54. The output of the SNSPDs was amplified, first, on the second cold stage using a two-stage HEMT (Eudyna FHX45X) preamplifier circuit and, second, with two room temperature coaxial amplifiers (MITEQ JS2100400-11-10P) followed by a thresholding circuit (Analog Circuits ADCMP58x) to convert the analog pulse to a digital signal.[55] The digital signals from both interferometer arms were collected with a time-correlated single photon counter (Picoquant Hydraharp 400). Data acquisition was performed using custom-made Labview routines. All of the data analysis including correlation of the photon streams was performed in MATLAB.

ASSOCIATED CONTENT

Supporting Information

The Supporting Information is available free of charge on the ACS Publications website at DOI: 10.1021/acsnano.8b07578.

Additional s-PCFS setup and sample characterization (PDF)

AUTHOR INFORMATION

Corresponding Author

*E-mail: mgb@mit.edu.

ORCID

Sophie N. Bertram: 0000-0002-9776-2284
Justin R. Caram: 0000-0001-5126-3829
Jason J. Yoo: 0000-0002-5773-1360
Moungi G. Bawendi: 0000-0003-2220-4365

Author Contributions

⊥S.N.B. and B.S. contributed equally to this work.

Notes

The authors declare no competing financial interest.

ACKNOWLEDGMENTS

This work is supported primarily by the Department of Energy (DOE) Office of Basic Energy Sciences, Division of Materials Sciences and Engineering (Award Number DE-FG02-07ER46454). R.M. (assisted with programming of the experiment-related equipment) and M.G. (performed maintenance of the SNSPDs) were supported through the DOE Center for Excitonics (an Energy Frontiers Research Center funded by the US DOE, through Grant DE-SC0001088). S.B. had additional government support through the National Science Foundation's Graduate Research Fellowship Program. D.F. (synthesized nanocrystals) was supported in part by the Boehringer Ingelheim Fonds and the NSF (Award Number EECS-1449291). J.Y. was supported by NASA NSTRF (Award Number NNX16AM70H).

REFERENCES

(1) Büning-Pfaue, H. Analysis of Water in Food by near Infrared Spectroscopy. *Food Chem.* **2003**, *82*, 107−115.

(2) Wilson, R. H.; Nadeau, K. P.; Jaworski, F. B.; Tromberg, B. J.; Durkin, A. J. Review of Short-Wave Infrared Spectroscopy and Imaging Methods for Biological Tissue Characterization. *J. Biomed. Opt.* **2015**, *20*, 030901.

(3) Hong, G.; Lee, J. C.; Robinson, J. T.; Raaz, U.; Xie, L.; Huang, N. F.; Cooke, J. P.; Dai, H. Multifunctional *in Vivo* Vascular Imaging Using Near-Infrared II Fluorescence. *Nat. Med.* **2012**, *18*, 1841.

(4) Diao, S.; Blackburn, J. L.; Hong, G.; Antaris, A. L.; Chang, J.; Wu, J. Z.; Zhang, B.; Cheng, K.; Kuo, C. J.; Dai, H. Fluorescence Imaging *In Vivo* at Wavelengths beyond 1500 Nm. *Angew. Chem., Int. Ed.* **2015**, *54*, 14758−14762.

(5) Steckel, J.; Coe-Sullivan, S.; Bulović, V.; Bawendi, M. 1.3μm to 1.55μm Tunable Electroluminescence from PbSe Quantum Dots Embedded within an Organic Device. *Adv. Mater.* **2003**, *15*, 1862−1866.

(6) Supran, G. J.; Song, K. W.; Hwang, G. W.; Correa, R. E.; Scherer, J.; Dauler, E. A.; Shirasaki, Y.; Bawendi, M. G.; Bulović, V. High-Performance Shortwave-Infrared Light-Emitting Devices Using Core−Shell (PbS−CdS) Colloidal Quantum Dots. *Adv. Mater.* **2015**, *27*, 1437−1442.

(7) Konstantatos, G.; Huang, C.; Levina, L.; Lu, Z.; Sargent, E. H. Efficient Infrared Electroluminescent Devices Using Solution-Processed Colloidal Quantum Dots. *Adv. Funct. Mater.* **2005**, *15*, 1865−1869.

(8) Sargent, E. H. Infrared Quantum Dots. *Adv. Mater.* **2005**, *17*, 515−522.

(9) Lee, J. W.; Kim, D. Y.; Baek, S.; Yu, H.; So, F. Inorganic UV−Visible−SWIR Broadband Photodetector Based on Monodisperse PbS Nanocrystals. *Small* **2016**, *12*, 1328−1333.

(10) Hu, C.; Gassenq, A.; Justo, Y.; Devloo-Casier, K.; Chen, H.; Detavernier, C.; Hens, Z.; Roelkens, G. Air-Stable Short-Wave Infrared PbS Colloidal Quantum Dot Photoconductors Passivated with Al $_2$O A$_3$tomic Layer Deposition. *Appl. Phys. Lett.* **2014**, *105*, 171110.

(11) McDonald, S. A.; Konstantatos, G.; Zhang, S.; Cyr, P. W.; Klem, E. J. D.; Levina, L.; Sargent, E. H. Solution-Processed PbS Quantum Dot Infrared Photodetectors and Photovoltaics. *Nat. Mater.* **2005**, *4*, 138−142.

(12) Dauler, E. A.; Grein, M. E.; Kerman, A. J.; Marsili, F.; Miki, S.; Nam, S. W.; Shaw, M. D.; Terai, H.; Verma, V. B.; Yamashita, T. Review of Superconducting Nanowire Single-Photon Detector System Design Options and Demonstrated Performance. *Opt. Eng.* **2014**, *53*, 081907.

(13) Boroson, D. M.; Robinson, B. S.; Murphy, D. V.; Burianek, D. A.; Khatri, F.; Kovalik, J. M.; Sodnik, Z.; Cornwell, D. M. Overview and Results of the Lunar Laser Communication Demonstration. *Proc. SPIE* **2014**, 89710S.

DOI: 10.1021/acsnano.8b07578
ACS Nano 2019, 13, 1042−1049

(14) McCarthy, A.; Krichel, N. J.; Gemmell, N. R.; Ren, X.; Tanner, M. G.; Dorenbos, S. N.; Zwiller, V.; Hadfield, R. H.; Buller, G. S. Kilometer-Range, High Resolution Depth Imaging *via* 1560 Nm Wavelength Single-Photon Detection. *Opt. Express* **2013**, *21*, 8904.
(15) Hadfield, R. H. Single-Photon Detectors for Optical Quantum Information Applications. *Nat. Photonics* **2009**, *3*, 696−705.
(16) Aharonovich, I.; Englund, D.; Toth, M. Solid-State Single-Photon Emitters. *Nat. Photonics* **2016**, *10*, 631−641.
(17) Ding, X.; He, Y.; Duan, Z.-C.; Gregersen, N.; Chen, M.-C.; Unsleber, S.; Maier, S.; Schneider, C.; Kamp, M.; Höfling, S.; Lu, C.-Y.; Pan, J.-W. On-Demand Single Photons with High Extraction Efficiency and Near-Unity Indistinguishability from a Resonantly Driven Quantum Dot in a Micropillar. *Phys. Rev. Lett.* **2016**, *116*, 020401.
(18) Riggs, J. E.; Guo, Z.; Carroll, D. L.; Sun, Y.-P. Strong Luminescence of Solubilized Carbon Nanotubes. *J. Am. Chem. Soc.* **2000**, *122*, 5879−5880.
(19) Tan, M. C.; Connolly, J.; Riman, R. E. Optical Efficiency of Short Wave Infrared Emitting Phosphors. *J. Phys. Chem. C* **2011**, *115*, 17952−17957.
(20) Hong, G.; Zou, Y.; Antaris, A. L.; Diao, S.; Wu, D.; Cheng, K.; Zhang, X.; Chen, C.; Liu, B.; He, Y.; Wu, J. Z.; Yuan, J.; Zhang, B.; Tao, Z.; Fukunaga, C.; Dai, H. Ultrafast Fluorescence Imaging *in Vivo* with Conjugated Polymer Fluorophores in the Second Near-Infrared Window. *Nat. Commun.* **2014**, *5*, 4206.
(21) Antaris, A. L.; Chen, H.; Cheng, K.; Sun, Y.; Hong, G.; Qu, C.; Diao, S.; Deng, Z.; Hu, X.; Zhang, B.; Zhang, X.; Yaghi, O. K.; Alamparambil, Z. R.; Hong, X.; Cheng, Z.; Dai, H. A Small-Molecule Dye for NIR-II Imaging. *Nat. Mater.* **2016**, *15*, 235−242.
(22) Thimsen, E.; Sadtler, B.; Berezin, M. Y. Shortwave-Infrared (SWIR) Emitters for Biological Imaging: A Review of Challenges and Opportunities. *Nanophotonics* **2017**, *6*, 1043.
(23) Semonin, O. E.; Johnson, J. C.; Luther, J. M.; Midgett, A. G.; Nozik, A. J.; Beard, M. C. Absolute Photoluminescence Quantum Yields of IR-26 Dye, PbS, and PbSe Quantum Dots. *J. Phys. Chem. Lett.* **2010**, *1*, 2445−2450.
(24) Weidman, M. C.; Beck, M. E.; Hoffman, R. S.; Prins, F.; Tisdale, W. A. Monodisperse, Air-Stable PbS Nanocrystals *via* Precursor Stoichiometry Control. *ACS Nano* **2014**, *8*, 6363−6371.
(25) Franke, D.; Harris, D. K.; Chen, O.; Bruns, O. T.; Carr, J. A.; Wilson, M. W. B.; Bawendi, M. G. Continuous Injection Synthesis of Indium Arsenide Quantum Dots Emissive in the Short-Wavelength Infrared. *Nat. Commun.* **2016**, *7*, 12749.
(26) Bruns, O. T.; Bischof, T. S.; Harris, D. K.; Franke, D.; Shi, Y.; Riedemann, L.; Bartelt, A.; Jaworski, F. B.; Carr, J. A.; Rowlands, C. J.; Wilson, M. W.; Chen, O.; Wei, H.; Hwang, G. W.; Montana, D. M.; Coropceanu, I.; Achorn, O. B.; Kloepper, J.; Heeren, J.; So, P. T. Next-Generation *in Vivo* Optical Imaging with Short-Wave Infrared Quantum Dots. *Nat. Biomed. Eng.* **2017**, *1*, 0056.
(27) Brackett, C. A. Dense Wavelength Division Multiplexing Networks: Principles and Applications. *IEEE J. Sel. Areas Commun.* **1990**, *8*, 948−964.
(28) Cui, J.; Beyler, A. P.; Coropceanu, I.; Cleary, L.; Avila, T. R.; Chen, Y.; Cordero, J. M.; Heathcote, S. L.; Harris, D. K.; Chen, O.; Cao, J.; Bawendi, M. G. Evolution of the Single-Nanocrystal Photoluminescence Linewidth with Size and Shell: Implications for Exciton−Phonon Coupling and the Optimization of Spectral Linewidths. *Nano Lett.* **2016**, *16*, 289−296.
(29) Nguyen, D. T.; Voisin, C.; Roussignol, P.; Roquelet, C.; Lauret, J. S.; Cassabois, G. Excitonic Homogeneous Broadening in Single-Wall Carbon Nanotubes. *Chem. Phys.* **2013**, *413*, 102−111.
(30) Ambrose, W. P.; Basché, T.; Moerner, W. E. Detection and Spectroscopy of Single Pentacene Molecules in a *p* -Terphenyl Crystal by Means of Fluorescence Excitation. *J. Chem. Phys.* **1991**, *95*, 7150−7163.
(31) Ha, T.; Ting, A. Y.; Liang, J.; Caldwell, W. B.; Deniz, A. A.; Chemla, D. S.; Schultz, P. G.; Weiss, S. Single-Molecule Fluorescence Spectroscopy of Enzyme Conformational Dynamics and Cleavage Mechanism. *Proc. Natl. Acad. Sci. U. S. A.* **1999**, *96*, 893−898.
(32) Sychugov, I.; Galeckas, A.; Elfström, N.; Wilkinson, A. R.; Elliman, R. G.; Linnros, J. Effect of Substrate Proximity on Luminescence Yield from Si Nanocrystals. *Appl. Phys. Lett.* **2006**, *89*, 111124.
(33) Li, Z. F.; Ruckenstein, E. Water-Soluble Poly(Acrylic Acid) Grafted Luminescent Silicon Nanoparticles and Their Use as Fluorescent Biological Staining Labels. *Nano Lett.* **2004**, *4*, 1463−1467.
(34) Marshall, L. F.; Cui, J.; Brokmann, X.; Bawendi, M. G. Extracting Spectral Dynamics from Single Chromophores in Solution. *Phys. Rev. Lett.* **2010**, *105*, 053005.
(35) Cox, I. J.; Sheppard, C. J. R. Information Capacity and Resolution in an Optical System. *J. Opt. Soc. Am. A* **1986**, *3*, 1152.
(36) Caram, J. R.; Bertram, S. N.; Utzat, H.; Hess, W. R.; Carr, J. A.; Bischof, T. S.; Beyler, A. P.; Wilson, M. W. B.; Bawendi, M. G. PbS Nanocrystal Emission Is Governed by Multiple Emissive States. *Nano Lett.* **2016**, *16*, 6070−6077.
(37) Correa, R. E.; Dauler, E. A.; Nair, G.; Pan, S. H.; Rosenberg, D.; Kerman, A. J.; Molnar, R. J.; Hu, X.; Marsili, F.; Anant, V.; Berggren, K. K.; Bawendi, M. G. Single Photon Counting from Individual Nanocrystals in the Infrared. *Nano Lett.* **2012**, *12*, 2953−2958.
(38) Bischof, T. S.; Correa, R. E.; Rosenberg, D.; Dauler, E. A.; Bawendi, M. G. Measurement of Emission Lifetime Dynamics and Biexciton Emission Quantum Yield of Individual InAs Colloidal Nanocrystals. *Nano Lett.* **2014**, *14*, 6787−6791.
(39) Peterson, J. J.; Krauss, T. D. Fluorescence Spectroscopy of Single Lead Sulfide Quantum Dots. *Nano Lett.* **2006**, *6*, 510−514.
(40) Muñoz-Matutano, G.; Barrera, D.; Fernández-Pousa, C.; Chulia-Jordan, R.; Seravalli, L.; Trevisi, G.; Frigeri, P.; Sales, S.; Martínez-Pastor, J. All-Optical Fiber Hanbury Brown & Twiss Interferometer to Study 1300 Nm Single Photon Emission of a Metamorphic InAs Quantum Dot. *Sci. Rep.* **2016**, *6*, 27214.
(41) Baiz, C. R.; Schach, D.; Tokmakoff, A. Ultrafast 2D IR Microscopy. *Opt. Express* **2014**, *22*, 18724.
(42) Barcik, P.; Wilfert, O.; Kolka, Z. Diffraction of the Optical Wave in the Schmidt Cassegrain Telescope. *Conf. Microwave Tech.* **2017**, 1−5.
(43) Harvey, J. E.; Ftaclas, C. Diffraction Effects of Telescope Secondary Mirror Spiders on Various Image-Quality Criteria. *Appl. Opt.* **1995**, *34*, 6337.
(44) Rosenberg, D.; Kerman, A. J.; Molnar, R. J.; Dauler, E. A. High-Speed and High-Efficiency Superconducting Nanowire Single Photon Detector Array. *Opt. Express* **2013**, *21*, 1440.
(45) Kimura, S.; Wilson, T. Confocal Scanning Optical Microscope Using Single-Mode Fiber for Signal Detection. *Appl. Opt.* **1991**, *30*, 2143.
(46) Allen, P. M.; Liu, W.; Chauhan, V. P.; Lee, J.; Ting, A. Y.; Fukumura, D.; Jain, R. K.; Bawendi, M. G. InAs(ZnCdS) Quantum Dots Optimized for Biological Imaging in the Near-Infrared. *J. Am. Chem. Soc.* **2010**, *132*, 470−471.
(47) Aharoni, A.; Mokari, T.; Popov, I.; Banin, U. Synthesis of InAs/CdSe/ZnSe Core/Shell1/Shell2 Structures with Bright and Stable Near-Infrared Fluorescence. *J. Am. Chem. Soc.* **2006**, *128*, 257−264.
(48) Kim, S.; Fisher, B.; Eisler, H.-J.; Bawendi, M. Type-II Quantum Dots: CdTe/CdSe(Core/Shell) and CdSe/ZnTe(Core/Shell) Heterostructures. *J. Am. Chem. Soc.* **2003**, *125*, 11466−11467.
(49) Mochizuki, K.; Namihira, Y.; Kuwazura, M.; Iwamoto, Y. Behavior of Hydrogen Molecules Adsorbed on Silica in Optical Fibers. *IEEE J. Quantum Electron.* **1984**, *20*, 694−697.
(50) Cui, J.; Beyler, A. P.; Marshall, L. F.; Chen, O.; Harris, D. K.; Wanger, D. D.; Brokmann, X.; Bawendi, M. G. Direct Probe of Spectral Inhomogeneity Reveals Synthetic Tunability of Single-Nanocrystal Spectral Linewidths. *Nat. Chem.* **2013**, *5*, 602−606.
(51) Lin, C.; Gong, K.; Kelley, D. F.; Kelley, A. M. Electron−Phonon Coupling in CdSe/CdS Core/Shell Quantum Dots. *ACS Nano* **2015**, *9*, 8131−8141.
(52) Lin, C.; Gong, K.; Kelley, D. F.; Kelley, A. M. Size-Dependent Exciton−Phonon Coupling in CdSe Nanocrystals through Resonance

DOI: 10.1021/acsnano.8b07578
ACS Nano 2019, 13, 1042−1049

Raman Excitation Profile Analysis. *J. Phys. Chem. C* **2015**, *119*, 7491−7498.
(53) Dzhagan, V. M.; Ya Valakh, M.; Raevskaya, A. E.; Stroyuk, A. L.; Kuchmiy, S. Y.; Zahn, D. R. T. Size Effects on Raman Spectra of Small CdSe Nanoparticles in Polymer Films. *Nanotechnology* **2008**, *19*, 305707.
(54) Dauler, E. A.; Kerman, A. J.; Robinson, B. S.; Yang, J. K.; Voronov, B.; Goltsman, G.; Hamilton, S. A.; Berggren, K. K. Photon-Number-Resolution with Sub-30-Ps Timing Using Multi-Element Superconducting Nanowire Single Photon Detectors. *J. Mod. Opt.* **2009**, *56*, 364−373.
(55) Kerman, A. J.; Rosenberg, D.; Molnar, R. J.; Dauler, E. A. Readout of Superconducting Nanowire Single-Photon Detectors at High Count Rates. *J. Appl. Phys.* **2013**, *113*, 144511.

DOI: 10.1021/acsnano.8b07578
ACS Nano 2019, 13, 1042−1049